



## Supporting Online Material for

### **Phase Separation of Lipid Membranes Analyzed with High-Resolution Secondary Ion Mass Spectrometry**

Mary L. Kraft, Peter K. Weber, Marjorie L. Longo, Ian D. Hutcheon, Steven G. Boxer\*

\*To whom correspondence should be addressed. E-mail: [sboxer@stanford.edu](mailto:sboxer@stanford.edu)

Published 29 September 2006, *Science* **313**, 1948 (2006)  
DOI: 10.1126/science.1130279

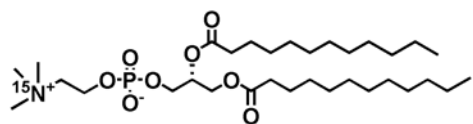
#### **This PDF file includes:**

Materials and Methods

Figs. S1 to S4

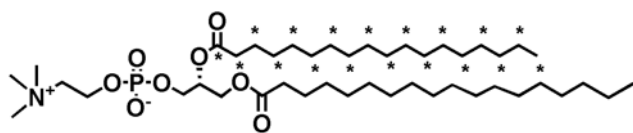
Tables S1 to S4

References

**Synthesis of isotopically labeled lipids**

**1)  $^{15}\text{N}$ -1,2-dilauryl-*sn*-glycero-3-phosphocholine:** Anhydrous pyridine (25 mL) was added to a flame-dried 50 mL 3-neck round bottom flask charged with  $^{15}\text{N}$ -choline chloride (449 mg, 3.192 mmol, Icon, Summit, NJ), 1,2-dilauryl-*sn*-glycero-3-phosphate (178 mg, 0.319 mmol, Avanti Polar Lipids Inc., Alabaster, AL) and a stir bar. Trichloroacetonitrile (5 mL) was slowly added to the flask, and the solution was placed in a 60 °C oil bath and stirred overnight. The solution was cooled, filtered to remove the precipitate, and concentrated via rotary evaporation under reduced pressure. To completely remove the pyridine, the brown residue was dissolved in 40 mL of  $\text{CH}_3\text{OH}$ - $\text{CHCl}_3$  (1:1) and concentrated via rotary evaporation under reduced pressure five times successively. Column chromatography on IWT TMD-8 ion exchange resin (50% tetrahydrofuran in water) yielded the product as a light brown wax. Column chromatography on silica gel ( $\text{CHCl}_3$ - $\text{CH}_3\text{OH}$ -water 65:25:4) produced the product as a beige wax that was re-purified by column chromatography on octadecyl-functionalized silica gel ( $\text{CHCl}_3$ - $\text{CH}_3\text{OH}$  1:9), yielding the pure phosphocholine (45.9 mg, 23.1%) as a white wax.  $^1\text{H}$  NMR ( $\text{CDCl}_3$ , 400 MHz)  $\delta$  5.19 (dd,  $J = 7.69, 12.2$  Hz, 1H), 4.38 (dd,  $J = 2.32, 12.01$  Hz, 1H), 4.31 (s, 2H), 4.11 (dd,  $J = 7.55, 12.12$  Hz, 1H), 3.93 (m, 2H), 3.8 (s, 2H), 3.35 (s, 9H), 2.30 (m, 2H), 1.57 (m, 4H), 1.25 (m, 32H), 0.87 (t,  $J = 6.79$  Hz, 6H);  $^{13}\text{C}$  NMR ( $\text{CDCl}_3$ , 400 MHz)  $\delta$  173.39 (d,  $J = 34.88$  Hz), 74.46, 70.352, 63.52, 62.868,

59.469, 54.34 (d,  $J = 5.42$  Hz), 34.30, 34.12, 31.91, 29.65, 29.55, 29.36, 29.19, 29.15, 24.96, 24.88, 22.27, 14.12. MS:  $[M + Na^+] = 645.2$



**2) 1-stearoyl-2-stearoyl- $^{13}C_{18}$ -sn-glycero-3-phosphocholine** was prepared in a two-step sequence: (i)  $^{13}C_{18}$ -stearoyl chloride. Anhydrous benzene (2 mL) was added to a flame-dried 15 mL 3-neck round bottom flask charged with  $^{13}C_{18}$ -stearic acid (96.5 mg, 0.3192 mmol, Isotec) and a stir bar. Oxalyl chloride (2.0 M in dichloromethane, 0.18 mL, 0.3510 mmol, Aldrich) was slowly added to the flask while stirring. After 1 h at rt, the flask was placed in a 60 °C oil bath and stirred overnight. The solution was cooled and concentrated via rotary evaporation, producing a yellow liquid that was used in the next reaction without further purification. (ii) To a stirred solution of 1-stearoyl-2-hydroxy *n*-glycero-3-phosphocholine (167 mg, 0.3192 mmol, Avanti Polar Lipids Inc., Alabaster, AL) and 4-dimethylaminopyridine (4 mg, 0.03192 mmol, Aldrich) dissolved in anhydrous chloroform (2 mL) were added anhydrous triethylamine (0.045 mL, 32.3 mmol) and  $^{13}C_{18}$ -stearoyl chloride (0.3192 mmol, assumed 100% yield) dissolved in anhydrous chloroform (3 mL). The resulting solution was stirred overnight at room temperature. Evaporation of the solvent followed by column chromatography on silica gel ( $CHCl_3$ - $CH_3OH$ -water 65:25:4) yielded the pure product (57.2 mg, 22.2% yield from  $^{13}C_{18}$ -stearic acid) as a white wax.  $^1H$  NMR ( $CDCl_3$ , 400 MHz)  $\delta$  5.18 (s, 1H), 4.37 (m, 1H), 4.25 (s, 2H), 4.11 (m, 1H), 3.90 (s, 2H), 3.71 (s 2H), 3.28 (s 9H), 2.32 (d,  $J = 128.74$

Hz, 2H), 2.26 (m, 2H), 1.55 (m, 2H), 1.55 (d,  $J = 131.86$  Hz, 2H), 1.24 (m, 28H), 1.24 (d,  $J = 118.69$  Hz, 28H), 0.88 (t,  $J = 6.83$  Hz, 3H), 0.87 (m, 3H);  $^{13}\text{C}$  NMR ( $\text{CDCl}_3$ , 400 MHz)  $\delta$  173.42 (dd,  $J = 57.15, 32.05$  Hz), 70.3, 66.41, 62.96, 60.09, 54.26, 34.19 (ddd,  $J = 57.34, 34.20, 17.80$  Hz), 31.92 (m), 29.75 (m), 24.96 (m), 22.67 (t,  $J = 34.96$  Hz), 14.11, 14.09 (d,  $J = 34.75$  Hz). MS:  $[\text{M} + \text{Cl}] = 842.2$

**Fabrication of substrates:** Oxidized silicon supports for these experiments were prepared with standard methods at the Stanford Nanofabrication Facility, as previously reported. Silicon wafers (4"  $\langle 100 \rangle$  *p*-type, Silicon Quest International, Santa Clara, CA,) were cleaned using a series of acid baths [10 min in  $\text{H}_2\text{SO}_4:\text{H}_2\text{O}$  (4:1) at 90 °C, rinse, 30 sec in  $\text{HF}:\text{H}_2\text{O}$  (1:50), rinse, 10 min in  $\text{H}_2\text{O}:\text{HCl}:\text{H}_2\text{O}_2$  (5:1:1) at 70°C, rinse, spin dry], and oxidized in a Tylan oxidation furnace (Tystar Corporation, Torrance, CA, 10 min at 1000 °C), producing a 17 nm-thick oxide layer, as determined by ellipsometry. This oxide thickness was selected as a compromise between maximal charge dissipation and secondary ion signal intensity during the SIMS analysis, and fluorescence signal intensity, which decreases with oxide thickness, for optical evaluation (see below). Chrome grid lines that were used as landmarks for sample positioning were formed on the oxidized wafers by coating the wafers with photoresist (Shipley 3612, 1.6  $\mu\text{m}$ -thick), photopatterning with UV light (Karl Suss MA-6 Contact Mask Aligner) through a chrome mask of a grid (Delta Mask), selectively removing the exposed resin, and depositing a thin film of chrome ( $\sim 5$  nm) over the uncovered oxide and remaining photoresist. Subsequent sonication in acetone removed the photoresist and the metal that

was deposited on top of it, but did not affect the chrome grid that was directly deposited on the oxidized substrate. The remaining chrome formed a grid that consisted of 10  $\mu\text{m}$ -wide bars positioned 50  $\mu\text{m}$  apart, thereby partitioning the surface of the oxidized substrate into a series of 40  $\mu\text{m}$  by 40  $\mu\text{m}$  squares. The patterned, oxidized wafers were cut into 5 mm by 5 mm squares for compatibility with the NanoSIMS sample holder using a conventional dicing saw, and cleaned by sonicating in acetone, washing with 7X detergent (ICN, Costa Mesa, CA, USA), and rinsing extensively with deionized water.

**Phase-Separated Supported Lipid Bilayers:** Chrome-patterned substrates were placed inside a 60 by 15 mm polystyrene culture dish and the dish and substrates were heated to 70 °C for ~ 45 min with a convection oven. While the substrates were heating, small unilamellar vesicles were prepared from mixtures of the isotopically labeled DSPC and DLPC, which was prepared as described above, and doped with 0.5 mol% of 1-palmitoyl-2-[12-(*N*-(7-nitrobenz-2-oxa-1,3-diazol-4-yl)amino)-caproyl]-*sn*-glycero-3-phosphocholine (12:0-*N*-NBD-PC, Avanti Polar Lipids, Alabaster, AL, USA) to facilitate verification of domain formation prior to NanoSIMS analysis and to evaluate the quality of the lipid bilayers after freeze-drying. A lipid mixture that contained an equal (mol) ratio of  $^{13}\text{C}_{18}$ -DSPC and  $^{15}\text{N}$ -DLPC was dissolved in chloroform, dried under a nitrogen stream, and placed under vacuum overnight to remove residual chloroform. The lipids were reconstituted with 1 mL of 70 °C Millipore (18 M $\Omega$ ) water, vortexed, and loaded into a mini-extruder (Avanti Polar Lipids). The assembled mini-extruder was placed into a 70 °C heating block and extruded through a 100 nm-pore polycarbonate membrane 19

times. The vesicle solution was diluted with 4 mL of 70 °C Millipore water, resulting in a final lipid concentration of 0.4 mg/mL. The vesicle solution was poured over the 70 °C substrates within the culture dish, the dish was covered to minimize evaporation, and incubated inside the 70 °C oven. After 1.5 h, the culture dish containing the substrates and vesicle solution was plunged into a 70 °C bowl of water in the oven to wash away the excess vesicles. The samples were slowly cooled to room temperature by gradually lowering the oven temperature to 50 °C over a period of 5 h, at which point the oven was shut off and the samples were allowed to cool to room temperature overnight.

**Supported Lipid Bilayers for Calibration of Lipid Content:** For each isotopically labeled lipid, a set of supported bilayer samples that systematically varied in isotopic enrichment was employed for calibration. Because the lipid bilayers used for calibration could not be phase-separated, the concentration of the isotopically labeled lipid was systematically varied through the addition of a second lipid component with a similar  $T_m$ .

*(i) Supported bilayers for calibration of  $^{15}\text{N}$ -DLPC:* Homogeneous lipid bilayers that systematically varied in their  $^{15}\text{N}$ -DLPC content [0, 20, 40, 60, 80, 98 mol%] were prepared to establish calibration curves. (We estimate that the error in the gravimetric measurements was less than 5 mol%.) For each homogeneous bilayer, 2 mol% 12:0-*N*-NBD-PC was added to the bilayer for optical inspection and rapid quality control, and 1,2-dioleoyl-*sn*-glycero-3-phosphocholine (DOPC, Avanti Polar Lipids Inc., Alabaster, AL, USA) made up the remaining mol% of lipid within the bilayer. The desired lipid

mixtures were dissolved in chloroform, dried under a nitrogen stream, exposed to vacuum overnight, and reconstituted with Millipore (18 M $\Omega$ ) water to a concentration of 3 mg/ml. Unilamellar vesicles were formed by passing the lipid suspension through a 50 nm-pore polycarbonate membrane 19 times. The extruded vesicles were stored at 4 °C and used within one week. Supported bilayers were formed by exposing the oxidized silicon substrate to the vesicle suspension, and rinsing in Millipore water to remove the excess vesicles. (ii) *Supported bilayers for calibration of  $^{13}\text{C}_{18}$ -DSPC*: Homogeneous lipid bilayers that systematically varied in their  $^{13}\text{C}_{18}$ -DSPC content [0, 20, 40, 60, 80, 98 mol%] were prepared to establish calibration curves. For each homogeneous bilayer, 2 mol% 12:0-*N*-NBD-PC was added to the bilayer for visualization, and unlabeled (natural abundance of  $^{13}\text{C}$  is 1.1%) 1,2-distearoyl-*sn*-glycero-3-phosphocholine (DSPC, Avanti Polar Lipids Inc., Alabaster, AL, USA) made up the remaining mol% of lipid within the bilayer. The desired lipid mixtures were dissolved in chloroform, dried under a nitrogen stream and maintained under vacuum for at least two hours to remove residual solvent. The lipids were reconstituted with enough 70 °C Millipore (18 M $\Omega$ ) water to make a lipid concentration of 3 mg/mL, vortexed, and loaded into a mini-extruder (Avanti Polar Lipids). The assembled mini-extruder was placed into a 70 °C heating block, and extruded through a 100 nm-pore polycarbonate membrane 19 times. A drop of the warm vesicle solution was deposited onto 70 °C chrome-patterned substrates, the substrates were rinsed in 70 °C water to remove the excess vesicles, and transferred to a container of room temperature water.

**Freeze-drying:** The samples were flash-frozen and freeze-dried as previously reported (1, 2) to preserve the organization of the lipid membranes on the length scale of the area sampled by the NanoSIMS during subsequent analysis. The substrates were carefully removed from the water bath such that a thin film of water remained on top of the bilayer, and quickly plunged into liquid ethane. The samples were transferred from the ethane into a pre-cooled drying chamber that was bathed in liquid nitrogen to keep the sample frozen throughout the drying process, and then subjected to reduced pressure (90  $\mu$ bar) generated by an oil-free scroll pump (Varian Inc., Lexington, MA, USA) equipped with a liquid nitrogen trap for a minimum of 12 h. Of note, lateral diffusion of the lipids within the bilayer ceased when the sample was freeze-dried, but could be resumed by re-hydrating the bilayer.

**Fluorescence Microscopy:** Although fluorophores are not required to identify the membrane composition using the NanoSIMS, their inclusion enables the use of fluorescence microscopy to evaluate the sample quality before and after freeze-drying, and to identify visual landmarks on the substrate that facilitate sample positioning for AFM and NanoSIMS characterization. A Nikon E800 fluorescence microscope equipped with a Photometrix Coolsnap HQ CCD camera and appropriate filter set was used to image the samples. Because 12:0-*N*-NBD-PC preferentially partitions into the fluid phase, gel phase domains were identified by their exclusion of 12:0-*N*-NBD-PC. A scribe was used to scratch the surface of the freeze-dried samples in the vicinity of corrals

that contained phase-separated lipid bilayers. A series of fluorescence microscopy images were taken to record the proximity of these corrals to the scratches, and these images were stitched together into a map of the sample.

**Freeze-drying control experiment:** To probe whether the freeze-drying process altered the lateral organization within the membrane, we investigated the size and location of phase-separated domains within a supported lipid membrane before and after freeze-drying. Because 12:0-*N*-NBD-PC is excluded from the gel phase domains, fluorescence microscopy can be employed to visualize phase separation within the sample. Phase-separated supported lipid membranes were made as described above but with slight modifications. The silicon substrates were oxidized to a thickness of 40 nm and patterned with a chrome grid that consisted of ~5  $\mu\text{m}$ -wide grid bars placed 25  $\mu\text{m}$  apart, dividing the substrate into ~20  $\mu\text{m}$  by 20  $\mu\text{m}$  squares. The substrates used in this experiment had a thicker SiO<sub>2</sub> layer (40 nm) than those used for the NanoSIMS experiments (17 nm) because bilayers supported on 17 nm-thick oxides exhibit substantially lower fluorescence intensity than that of samples supported by a 40 nm-thick oxide layer due to destructive interference from reflection off the silicon mirror. This change in the oxide thickness does not affect the freeze-drying process. The lipid membrane was composed of an equal molar ratio of unlabeled DLPC and DSPC (Avanti Polar Lipids), and the amount of 12:0-*N*-NBD-PC was increased to 2 mol% to compensate for photobleaching induced by the more extensive sample imaging. Scratches made on the surface of the hydrated phase-separated supported lipid bilayers

using a diamond scribe served as landmarks that enabled the unambiguous relocation of the same sample position at a later time. The samples were freeze-dried as described and re-imaged with fluorescence microscopy. Phase-separated regions of the supported lipid bilayer showed that the size, shape, and position of the microdomains were nearly identical before and after freeze-drying (Fig. S1), indicating the lateral organization within the membrane was essentially unchanged by the freeze-drying process.

**AFM imaging:** The topography of the freeze-dried lipid bilayers was imaged in ambient air with a Nanoscope III AFM (Digital Instruments Inc., Santa Barbara, CA, USA). Measurements were performed in tapping mode with a J scan head. All scans were performed with silicon non-contact, high resonance frequency cantilevers, model TESP (Veeco, Santa Barbara, CA). AFM imaging was performed on corrals that contained phase-separated lipid bilayers, which were located using the fluorescence microscopy images described, *vide supra*. Because comparison between AFM and NanoSIMS images was desired, the specific corrals imaged by AFM were noted on the fluorescence map of the sample. Because 512 by 512 pixel images were acquired of relatively large (35  $\mu\text{m}$  by 35  $\mu\text{m}$ ) areas of the sample in order to identify regions for NanoSIMS analysis, the lateral resolution of these AFM images is limited by the pixel-to-area ratio, and is therefore significantly lower than that obtainable with AFM.

**Secondary Ion Mass Spectrometry (SIMS):** SIMS was performed using the Lawrence Livermore National Laboratory NanoSIMS 50. The measurements were made with a  $\sim 4$  pA, 16 keV  $^{133}\text{Cs}^+$  primary ion beam focused into a  $\sim 90$  nm diameter spot (see below) and rastered over sample areas that were 25  $\mu\text{m}$  by 25  $\mu\text{m}$ . The isotope imaging measurements consist of 10 replicate scans of 256 by 256 pixels with a dwell time of 0.5 ms/pixel. Secondary ion intensities for  $^{12}\text{C}^-$ ,  $^{13}\text{C}^-$ ,  $^{13}\text{C}^1\text{H}^-$ ,  $^{12}\text{C}^{15}\text{N}^-$ , and  $^{31}\text{P}^-$  were collected simultaneously in multi-collection mode. A mass resolving power of  $\sim 6800$  was used to separate isobaric interferences from the isotopes of interest, e.g.,  $^{13}\text{C}^1\text{H}$  from  $^{12}\text{C}^1\text{H}_2$  at mass 14, and  $^{12}\text{C}^{15}\text{N}$  from  $^{13}\text{C}^{14}\text{N}$  at mass 27. Samples were also simultaneously imaged using secondary electrons. The corrals that were imaged by AFM were first visually located with a CCD camera using the fluorescence microscopy images, then were moved to the analysis position in the NanoSIMS and precisely positioned using real-time secondary electron imaging.

**Determination of Primary  $\text{Cs}^+$  Beam Spot Size:** The knife-edge method was used to determine the lateral resolution of the SIMS images. The beam diameter was determined as the distance over which the secondary electron intensity increased from 16% to 84% of the maximum, measured on a line scan taken at a sample location where there was a sharp change in the composition of the sample. A beam spot size of 87 nm was measured (Fig. S2). The lateral resolution in the NanoSIMS images depends on both the size of the primary ion beam and the size of the pixels in the image. Because the pixel size in the images (97 nm) was greater than the ion beam spot size, the best lateral resolution of

these NanoSIMS images is 97 nm. The quantitative NanoSIMS images (Fig. 3) were acquired with the same pixel and spot size, and a three pixel wide boxcar-smoothing algorithm was applied to the data.

**Data Analysis:** Data analysis was performed using custom software (LIMAGE, L.R. Nittler), which runs on the PV-WAVE platform (Visual Numerics, Inc., Houston, TX). The NanoSIMS secondary ion intensities were normalized to  $^{12}\text{C}^-$  in order to minimize systematic signal intensity variations that arose during the measurements. Each image of the normalized  $^{13}\text{C}^{1}\text{H}^-$  or  $^{12}\text{C}^{15}\text{N}^-$  intensities was smoothed with a 3-pixel window for noise reduction.

**Quantitative Analysis of Lipid Content:** To establish calibration curves for the isotopically labeled lipids, sets of homogeneous samples that systematically varied in the mol%  $^{13}\text{C}_{18}$ -DSPC or  $^{15}\text{N}$ -DLPC (described above) were analyzed by the NanoSIMS. Several regions were selected on each homogeneous sample of a specified mol%  $^{13}\text{C}_{18}$ -DSPC or  $^{15}\text{N}$ -DLPC such that the region bounded an area covered by membrane within a single grid box, but did not include secondary ion signals originating from the chrome grid or obvious defects in the bilayer. The normalized  $^{13}\text{C}^{1}\text{H}^-$  or  $^{12}\text{C}^{15}\text{N}^-$  signal ( $^{13}\text{C}^{1}\text{H}^- / ^{12}\text{C}^-$  or  $^{12}\text{C}^{15}\text{N}^- / ^{12}\text{C}^-$ , respectively) was determined for each region. The data for each mol% of isotopically labeled lipid were tabulated, and the mean values of the normalized signals were determined for each specified mol% using standard statistical analysis methods.

Although the normalized secondary ion signal is correlated to the mol% of isotopically labeled lipid in the membrane, the lipid mixtures used for the calibration samples contained more natural abundance carbon atoms than the lipid mixtures used to make the phase-separated bilayers. The bilayer samples used to calibrate  $^{13}\text{C}_{18}$ -DSPC contained variable mol ratios of  $^{13}\text{C}_{18}$ -DSPC and DSPC (with 0.5 mol% 12:0-*N*-NBD-PC), which contain 26, 44, and 42 unlabeled carbon atoms. The samples used to calibrate the  $^{15}\text{N}$ -DLPC content contained variable mol ratios of  $^{15}\text{N}$ -DLPC and DOPC with 0.5 mol% 12:0-*N*-NBD-PC, which consist of 32, 44, and 42 unlabeled carbon atoms. The phase-separated lipid bilayers were made of  $^{13}\text{C}_{18}$ -DSPC,  $^{15}\text{N}$ -DLPC, and 12:0-*N*-NBD-PC, which contained 26, 32, and 42 unlabeled carbon atoms. As a result, for a given mol% of isotopically labeled lipid, the isotopic composition of the lipid mixture in the calibration samples, which is expressed as the ratio of isotopically labeled atoms to unlabeled carbons (e.g.,  $^{13}\text{C}/^{12}\text{C}$  or  $^{15}\text{N}/^{12}\text{C}$ ) in the lipid mixture and is determined from the structures of the lipids within the sample, differed from that of the phase-separated samples. For example, a 1:1  $^{13}\text{C}_{18}$ -DSPC: DSPC mixture has a  $^{13}\text{C}/^{12}\text{C}$  ratio of 9/35; whereas a 1:1  $^{13}\text{C}_{18}$ -DSPC:  $^{15}\text{N}$ -DLPC has a  $^{13}\text{C}/^{12}\text{C}$  value of 9/29. Therefore the normalized secondary ion signal was plotted against the mixture's specific isotopic composition (Fig. S3), which can be used to determine the amount of isotopically labeled lipid within the phase-separated lipid bilayers. Table S1 summarizes the correlation between the isotopic enrichment and the mol%  $^{13}\text{C}_{18}$ -DSPC for the  $^{13}\text{C}_{18}$ -DSPC calibration samples. The best-fit line was determined by linear regression. A two-step calculation was then used to deduce the mol% of  $^{13}\text{C}_{18}$ -DSPC and  $^{15}\text{N}$ -DLPC in regions

of interest on the domain samples, where the amount of each lipid was independently determined. First, the calibration curves described above were used to correlate the normalized  $^{13}\text{C}^1\text{H}^-$  and  $^{12}\text{C}^{15}\text{N}^-$  signals ( $^{13}\text{C}^1\text{H}^-/^{12}\text{C}^-$  or  $^{12}\text{C}^{15}\text{N}^-/^{12}\text{C}^-$ , respectively) collected from a specific region of the bilayer to the isotopic composition (i.e.,  $^{13}\text{C}/^{12}\text{C}$  or  $^{15}\text{N}/^{12}\text{C}$ ) of the lipids located in that area. The mol% of isotopically labeled lipid that corresponds to this isotopic composition was determined from the structures of the lipid components, as described above, assuming the presence of 0.5 mol% 12:0-*N*-NBD-PC throughout the bilayer. This assumption may introduce a small amount of error in the estimation because the distribution of 12:0-*N*-NBD-PC is heterogeneous, however given the small amount of 12:0-*N*-NBD-PC in the mixture, this error is insignificant.

To assess whether there were statistically significant variations in the lipid composition within the gel phase domains shown in Fig. 3, each domain was divided into 3 by 3 pixel regions of interest (ROI), where each ROI encompassed only the gel phase and did not contain debris or the domain perimeter. The amount of  $^{15}\text{N}$ -DLPC within each ROI was determined from the  $^{12}\text{C}^{15}\text{N}^-/^{12}\text{C}^-$  NanoSIMS secondary ion intensity by calculating the  $^{15}\text{N}/^{12}\text{C}$  ratio for the mixture, as described above; the mol% of  $^{15}\text{N}$ -DLPC was then calculated from this value. The amount of  $^{13}\text{C}_{18}$ -DSPC was determined in a similar manner from the  $^{13}\text{C}^1\text{H}^-/^{12}\text{C}^-$  secondary ion intensity ratio. The  $^{15}\text{N}$ -DLPC and  $^{13}\text{C}_{18}$ -DSPC content within the ROI was normalized so the total lipid content was 100%, and the uncertainty ( $\sigma$ ) in the measurement was calculated using Poisson statistics uncertainties (counting statistics) (Eq. 1) and propagating those uncertainties in quadrature (Eq. 2) (see Table S2-S4 for more details):

$$(1) \quad \sigma_{counting\ stats} = \sqrt{NanoSIMS\ intensity_{cts}}$$

$$(2) \quad \sigma_{Normalized\ ion\ intensity} = \left( \frac{ion\ intensity_{cts}}{^{12}C_{cts}^-} \right) \cdot \sqrt{\left[ \left( \frac{\sqrt{ion\ intensity_{cts}}}{ion\ intensity_{cts}} \right)^2 + \left( \frac{\sqrt{^{12}C_{cts}^-}}{^{12}C_{cts}^-} \right)^2 \right]}$$

The location of the ROIs within the domains and the normalized mol% of  $^{15}\text{N}$ -DLPC and  $^{13}\text{C}_{18}$ -DSPC for each ROI is shown in Fig. S4.

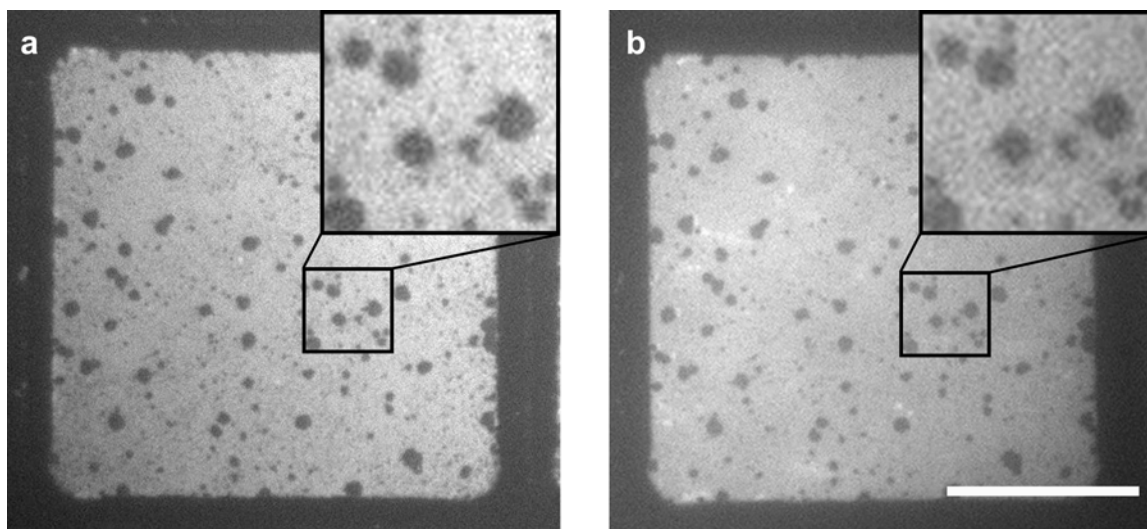


**Figure S1.** Fluorescence microscopy images of a phase-separated DLPC and DSPC lipid bilayer doped with 2 mol% 12:0-*N*-NBD-PC assembled on chrome-patterned oxidized silicon (a) before and (b) after freeze-drying. The chrome grid is visible as a dark square around the edges of the images, and an enlarged image of the region outlined in black is provided in the inset. Reduced contrast in the freeze-dried image is due to the lower fluorescence intensity of the dehydrated sample. Fluorescently labeled lipids are excluded from the gel-phase domains, which appear dark. Following freeze-drying, the size, shape, and positions of the individual domains appeared virtually identical to those imaged while the sample was hydrated. Scale bar is 10  $\mu\text{m}$ .

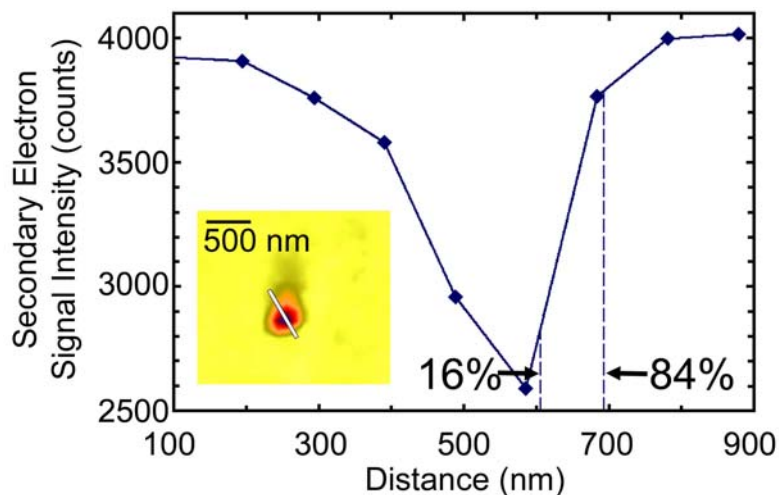


**Figure S2.** A primary  $\text{Cs}^+$  beam spot size of 87 nm was determined by measuring the distance over which the secondary electron signal intensity increased from 16% to 84% of the maximum along a line scan acquired at a sharp composition boundary between debris on the sample and the neighboring bilayer (inset). A spot size of  $\sim 90$  nm in diameter was measured based on this criterion; the lateral resolution of the SIMS images is somewhat lower because the pixel size is  $\sim 100$  nm by 100 nm.

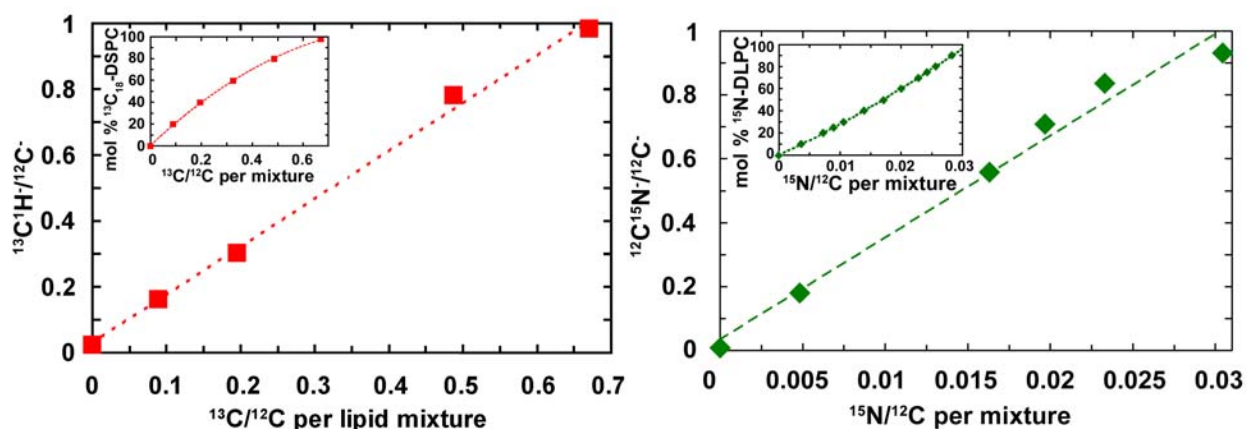


**Figure S3.** Calibration curves showing the correlation between the normalized  $^{13}\text{C}^1\text{H}^-$  or  $^{12}\text{C}^{15}\text{N}^-$  ( $^{13}\text{C}^1\text{H}/^{12}\text{C}^-$  or  $^{12}\text{C}^{15}\text{N}/^{12}\text{C}^-$ ) secondary ion signal and the isotopic composition ( $^{13}\text{C}/^{12}\text{C}$  or  $^{15}\text{N}/^{12}\text{C}$ ) of the lipid mixture. Curves were constructed from NanoSIMS measurements made on sets of homogeneous bilayers that systematically varied in the mol% of  $^{13}\text{C}_{18}$ -DSPC or  $^{15}\text{N}$ -DLPC. We estimate that the error in the gravimetric measurements were less than 5%. Because simple lipid mixtures were employed, each isotopic composition corresponds to a specific mol% of  $^{13}\text{C}_{18}$ -DSPC or  $^{15}\text{N}$ -DLPC in the sample (insets). Table S1 describes how the isotopic enrichment is calculated for different lipid mixtures.

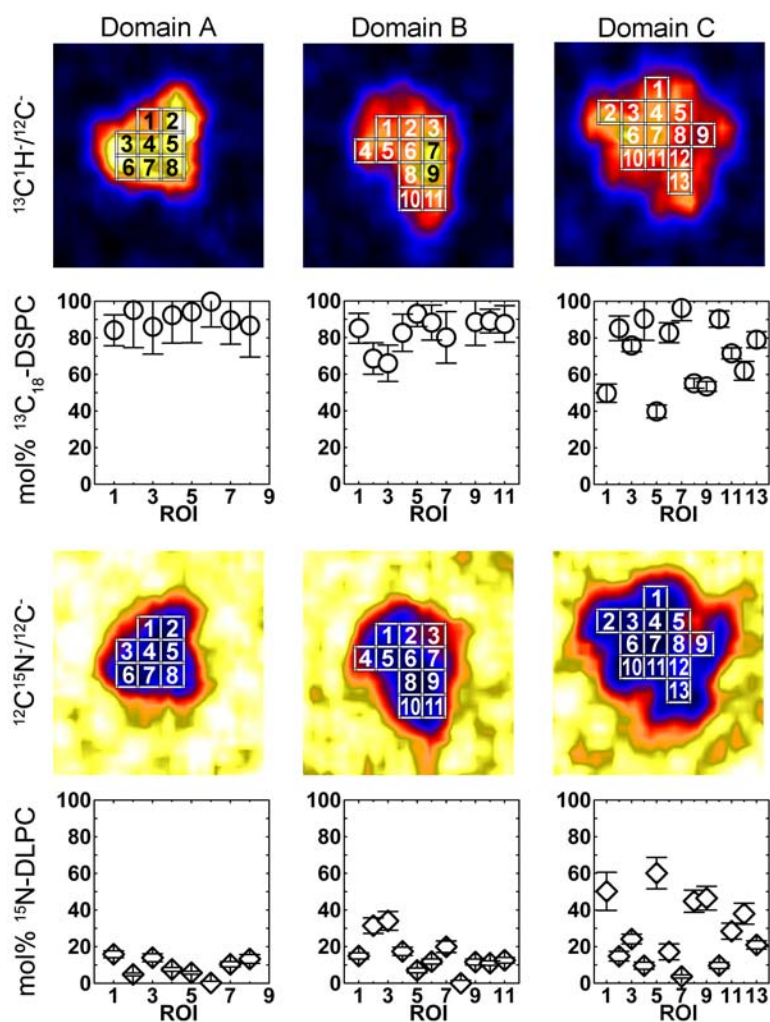


**Figure S4.** Quantitative analysis of the gel phase domains shown in Fig. 3. Each domain was divided into 3 by 3 pixel regions, and the specific locations of these ROIs within the domains are shown on the NanoSIMS images, and are identical to those shown in Fig. 4. Graphs illustrate the mol%  $^{15}\text{N}$ -DLPC and  $^{13}\text{C}_{18}$ -DSPC determined from the NanoSIMS secondary ion intensities detected at each ROI, where the mol%  $^{15}\text{N}$ -DLPC and  $^{13}\text{C}_{18}$ -DSPC are displayed in separate graphs for simplicity.

**Table S1. Calculation of Theoretical  $^{13}\text{C}/^{12}\text{C}$  Isotopic Enrichment Values <sup>a</sup>**

mol% $^{13}\text{C}_{18}$ - DSPC	Unlabeled carbon atoms from:			Total unlabeled carbon atoms	$^{13}\text{C}$ atoms from $^{13}\text{C}_{18}$ - DSPC <sup>e</sup>	$^{13}\text{C}$ /unlabeled carbon atoms
	$^{13}\text{C}_{18}$ -DSPC <sup>b</sup>	NBD-PC <sup>c</sup>	DSPC <sup>d</sup>			
0	0	0.84	43.1	43.9	0	0
20	5.2	0.84	34.3	40.3	3.6	0.0892
40	10.4	0.84	25.5	36.7	7.2	0.196
60	15.6	0.84	16.7	33.1	10.8	0.326
80	20.8	0.84	7.9	29.5	14.4	0.487
98	25.5	0.84	0	26.3	17.6	0.670

<sup>a</sup> Similar tables were constructed to correlate the isotopic composition to the  $^{13}\text{C}_{18}$ -DSPC or  $^{15}\text{N}$ -DLPC mol% in the domain samples using the structures of the lipid components within the bilayer

<sup>b</sup> = mol ratio of  $^{13}\text{C}_{18}$ -DSPC  $\cdot$  26; 26 is the number of unlabeled carbon atoms in the molecule mol ratio of  $^{13}\text{C}_{18}$ -DSPC  $\cdot$  18. A plot of the mol%  $^{13}\text{C}_{18}$ -DSPC versus the isotopic composition is created from this data, as shown in Fig. S3 left inset

<sup>c</sup> = mol ratio of NBD-PC  $\cdot$  42; the mol ratio is 0.02, and 42 is the number of unlabeled carbon atoms in the molecule

<sup>d</sup> = mol ratio of DSPC  $\cdot$  44; 44 is the number of unlabeled carbon atoms in the molecule

<sup>e</sup> = mol ratio of  $^{13}\text{C}_{18}$ -DSPC  $\cdot$  18. A plot of the mol%  $^{13}\text{C}_{18}$ -DSPC versus the isotopic composition is created from this data, as shown in Fig. S3 left inset

**Table S2. Domain A Calculations**

ROI	$^{13}\text{C}^1\text{H}^-$ cts	$^{12}\text{C}^-$ cts	$^{13}\text{C}^1\text{H}/^{12}\text{C}^-$	uncertainty $^{13}\text{C}^1\text{H}/^{12}\text{C}^-$ <sup>a</sup>	$^{13}\text{C}/^{12}\text{C}$ <sup>b</sup>	uncertainty $^{13}\text{C}/^{12}\text{C}$ <sup>c</sup>	calc mol% $^{13}\text{C}_{18}\text{-DSPC}$ <sup>d</sup>	uncertainty mol% $^{13}\text{C}_{18}\text{-DSPC}$ <sup>e</sup>
1	53	110	$4.82 \times 10^{-1}$	$8.06 \times 10^{-2}$	$3.10 \times 10^{-1}$	$3.64 \times 10^{-2}$	49.8	8.5
2	87	86	1.01	$1.54 \times 10^{-1}$	$6.72 \times 10^{-1}$	$8.65 \times 10^{-2}$	97.6	20.5
3	77	96	$8.02 \times 10^{-1}$	$1.23 \times 10^{-1}$	$5.29 \times 10^{-1}$	$6.52 \times 10^{-2}$	79.9	14.9
4	79	98	$8.06 \times 10^{-1}$	$1.22 \times 10^{-1}$	$5.32 \times 10^{-1}$	$6.47 \times 10^{-2}$	80.3	15.3
5	82	94	$8.72 \times 10^{-1}$	$1.32 \times 10^{-1}$	$5.77 \times 10^{-1}$	$7.14 \times 10^{-2}$	86.1	16.9
6	60	91	$6.59 \times 10^{-1}$	$1.10 \times 10^{-1}$	$4.32 \times 10^{-1}$	$5.63 \times 10^{-2}$	67.0	13.9
7	63	94	$6.70 \times 10^{-1}$	$1.09 \times 10^{-1}$	$4.39 \times 10^{-1}$	$5.59 \times 10^{-2}$	68.0	13.1
8	73	85	$8.59 \times 10^{-1}$	$1.37 \times 10^{-1}$	$5.68 \times 10^{-1}$	$7.50 \times 10^{-2}$	84.9	17.2

$$^a \sigma_{\frac{^{13}\text{C}^1\text{H}_{\text{cts}}^-}{^{12}\text{C}_{\text{cts}}^-}} = \left( \frac{^{13}\text{C}^1\text{H}_{\text{cts}}^-}{^{12}\text{C}_{\text{cts}}^-} \right) \cdot \sqrt{\left[ \left( \frac{\sqrt{^{13}\text{C}^1\text{H}_{\text{cts}}^-}}{^{13}\text{C}^1\text{H}_{\text{cts}}^-} \right)^2 + \left( \frac{\sqrt{^{12}\text{C}_{\text{cts}}^-}}{^{12}\text{C}_{\text{cts}}^-} \right)^2 \right]}$$

$$^b \frac{^{13}\text{C}_{\text{atoms}}}{^{12}\text{C}_{\text{atoms}}} = \left[ \left( \frac{^{13}\text{C}^1\text{H}_{\text{cts}}^-}{^{12}\text{C}_{\text{cts}}^-} \right) - 0.272 \right] / 1.4643; \text{ equation is the best fit line of the } ^{13}\text{C}_{18}\text{-DSPC calibration graph Fig. S3)}$$

$$^c \sigma_{\frac{^{13}\text{C}_{\text{atoms}}}{^{12}\text{C}_{\text{atoms}}}} = \left[ \left( \sigma_{\frac{^{13}\text{C}^1\text{H}_{\text{cts}}^-}{^{12}\text{C}_{\text{cts}}^-}} \right) - 0.272 \right] / 1.4643$$

$$^d \text{calc mol\% } ^{13}\text{C}_{18}\text{-DSPC} = \left[ -40.523 \cdot \left( \frac{^{13}\text{C}_{\text{atoms}}}{^{12}\text{C}_{\text{atoms}}} \right) \right] + \left[ 172.06 \cdot \left( \frac{^{13}\text{C}_{\text{atoms}}}{^{12}\text{C}_{\text{atoms}}} \right) \right] + 0.2424; \text{ equation is the best fit line of the inset graph in the left side of Fig. S3}$$

$$^e \sigma_{\text{calc mol\% } ^{13}\text{C}_{18}\text{-DSPC}} = \left[ -40.523 \cdot \left( \sigma_{\frac{^{13}\text{C}_{\text{atoms}}}{^{12}\text{C}_{\text{atoms}}}} \right) \right] + \left[ 172.06 \cdot \left( \sigma_{\frac{^{13}\text{C}_{\text{atoms}}}{^{12}\text{C}_{\text{atoms}}}} \right) \right] + 0.2424$$

ROI	$^{12}\text{C}^{15}\text{N}^-$ cts	$^{12}\text{C}^-$ cts	$^{12}\text{C}^{15}\text{N}^-/^{12}\text{C}^-$	uncertainty $^{12}\text{C}^{15}\text{N}^-/^{12}\text{C}^-$ f	$^{15}\text{N}/^{12}\text{C}$ g	uncertainty $^{15}\text{N}/^{12}\text{C}$ h	calc mol% $^{15}\text{N-DLPC}$ i	uncertainty mol% $^{15}\text{N-DLPC}$ j
1	16	110	$1.45 \times 10^{-1}$	$3.89 \times 10^{-2}$	$3.51 \times 10^{-3}$	$1.79 \times 10^{-4}$	9.4	0.6
2	8	86	$9.30 \times 10^{-2}$	$3.44 \times 10^{-2}$	$1.87 \times 10^{-3}$	$3.71 \times 10^{-5}$	5.0	0.2
3	18	96	$1.88 \times 10^{-1}$	$4.82 \times 10^{-2}$	$4.83 \times 10^{-3}$	$4.68 \times 10^{-4}$	13.0	1.4
4	11	98	$1.12 \times 10^{-1}$	$3.57 \times 10^{-2}$	$2.47 \times 10^{-3}$	$7.80 \times 10^{-5}$	6.6	0.4
5	9	94	$9.57 \times 10^{-2}$	$3.34 \times 10^{-2}$	$1.96 \times 10^{-3}$	$6.50 \times 10^{-6}$	5.2	0.2
6	3	91	$3.30 \times 10^{-2}$	$1.93 \times 10^{-2}$	$7.29 \times 10^{-6}$	$4.33 \times 10^{-4}$	0.1	0.9
7	12	94	$1.28 \times 10^{-1}$	$3.91 \times 10^{-2}$	$2.96 \times 10^{-3}$	$1.86 \times 10^{-4}$	7.9	0.6
8	16	85	$1.88 \times 10^{-1}$	$5.13 \times 10^{-2}$	$4.85 \times 10^{-3}$	$5.66 \times 10^{-4}$	13.0	1.6

$$f \quad \sigma_{\frac{^{12}\text{C}^{15}\text{N}^-}{^{12}\text{C}^-}} = \left( \frac{^{12}\text{C}^{15}\text{N}^-}{^{12}\text{C}^-} \right) \cdot \sqrt{\left[ \left( \frac{\sqrt{^{12}\text{C}^{15}\text{N}^-}}{^{12}\text{C}^{15}\text{N}^-} \right)^2 + \left( \frac{\sqrt{^{12}\text{C}^-}}{^{12}\text{C}^-} \right)^2 \right]}$$

$$g \quad \frac{^{15}\text{N}_{atoms}}{^{12}\text{C}_{atoms}} = \left[ \left( \frac{^{12}\text{C}^{15}\text{N}^-}{^{12}\text{C}^-} \right) - 0.0332 \right] / 31.964 \text{ equation is the best-fit line of the } ^{15}\text{N-DLPC calibration graph (fig. S3)}$$

$$h \quad \sigma_{\frac{^{15}\text{N}_{atoms}}{^{12}\text{C}_{atoms}}} = \left[ \left( \sigma_{\frac{^{12}\text{C}^{15}\text{N}^-}{^{12}\text{C}^-}} \right) - 0.0332 \right] / 31.964$$

$$i \quad \text{calc mol\% } ^{15}\text{N-DLPC} = \left[ 21192 \cdot \left( \frac{^{15}\text{N}_{atoms}}{^{12}\text{C}_{atoms}} \right) \right]^2 + \left[ 2551.2 \cdot \left( \frac{^{15}\text{N}_{atoms}}{^{12}\text{C}_{atoms}} \right) \right] + 0.1552$$

$$j \quad \sigma_{\text{calc mol\% } ^{15}\text{N-DLPC}} = \left[ 21192 \cdot \left( \sigma_{\frac{^{15}\text{N}_{atoms}}{^{12}\text{C}_{atoms}}} \right) \right]^2 + \left[ 2551.2 \cdot \left( \sigma_{\frac{^{15}\text{N}_{atoms}}{^{12}\text{C}_{atoms}}} \right) \right] + 0.1552$$

ROI	calc mol% $^{13}\text{C}_{18}$ -DSPC	calc mol% $^{15}\text{N}$ -DLPC	total calc mol% lipid	normalized $^{13}\text{C}_{18}$ -DSPC <sup>k</sup>	uncertainty normalized $^{13}\text{C}_{18}$ -DSPC <sup>l</sup>	normalized $^{15}\text{N}$ -DLPC <sup>m</sup>	uncertainty normalized $^{15}\text{N}$ -DLPC <sup>n</sup>
1	49.8	9.4	59.1	84	8.5	16	1.8
2	97.6	5.0	102.6	95	20.5	5	0.7
3	79.9	13.0	92.9	86	14.9	14	2.2
4	80.3	6.6	86.9	92	15.3	8	1.0
5	86.1	5.2	91.3	94	16.9	6	0.8
6	67.0	0.1	67.1	100	13.9	0	0.9
7	68.0	7.9	75.9	90	13.1	10	1.5
8	84.9	13.0	97.9	87	17.2	13	2.4

Table S3. Domain B Calculations

ROI	$^{13}\text{C}^1\text{H}^-$ cts	$^{12}\text{C}^-$ cts	$^{13}\text{C}^1\text{H}/^{12}\text{C}^-$	uncertainty $^{13}\text{C}^1\text{H}/^{12}\text{C}^-$	$^{13}\text{C}/^{12}\text{C}$	uncertainty $^{13}\text{C}/^{12}\text{C}$	calc mol% $^{13}\text{C}_{18}$ -DSPC	uncertainty mol% $^{13}\text{C}_{18}$ -DSPC
1	60	121	$4.96 \times 10^{-1}$	$7.83 \times 10^{-2}$	$3.20 \times 10^{-1}$	$3.49 \times 10^{-2}$	51.2	6.2
2	59	112	$5.27 \times 10^{-1}$	$8.47 \times 10^{-2}$	$3.41 \times 10^{-1}$	$3.93 \times 10^{-2}$	54.2	6.9
3	54	97	$5.57 \times 10^{-1}$	$9.45 \times 10^{-2}$	$3.62 \times 10^{-1}$	$4.60 \times 10^{-2}$	57.2	8.1
4	71	116	$6.12 \times 10^{-1}$	$9.22 \times 10^{-2}$	$3.99 \times 10^{-1}$	$4.44 \times 10^{-2}$	62.5	7.8
5	60	135	$4.44 \times 10^{-1}$	$6.90 \times 10^{-2}$	$2.85 \times 10^{-1}$	$2.85 \times 10^{-2}$	46.0	5.1
6	62	113	$5.49 \times 10^{-1}$	$8.67 \times 10^{-2}$	$3.56 \times 10^{-1}$	$4.06 \times 10^{-2}$	56.4	7.2
7	78	99	$7.88 \times 10^{-1}$	$1.19 \times 10^{-1}$	$5.19 \times 10^{-1}$	$6.29 \times 10^{-2}$	78.7	10.9
8	68	101	$6.73 \times 10^{-1}$	$1.06 \times 10^{-1}$	$4.41 \times 10^{-1}$	$5.35 \times 10^{-2}$	68.3	9.3

$$^k \text{ normalized mol\% } ^{13}\text{C}_{18} - \text{DSPC} = \left( \frac{\text{calc mol\% } ^{13}\text{C}_{18} - \text{DSPC}}{\text{total calc mol\% lipid}} \right) \cdot 100$$

l

$$^{\sigma} \text{ normalized mol\% } ^{13}\text{C}_{18} - \text{DSPC} =$$

$$\text{calc mol\% } ^{13}\text{C}_{18} - \text{DSPC} \cdot \sqrt{\left[ \frac{\sigma_{\text{calc mol\% } ^{13}\text{C}_{18} - \text{DSPC}}}{\text{calc mol\% } ^{13}\text{C}_{18} - \text{DSPC}} \right]^2 + \left[ \frac{\sqrt{[(\sigma_{\text{calc mol\% } ^{15}\text{N} - \text{DLPC}})^2 + (\sigma_{\text{calc mol\% } ^{13}\text{C}_{18} - \text{DSPC}})^2]}}{\text{total calc mol\% lipid}} \right]^2}$$

$$^m \text{ normalized mol\% } ^{15}\text{N} - \text{DLPC} = \left( \frac{\text{calc mol\% } ^{15}\text{N} - \text{DLPC}}{\text{total calc mol\% lipid}} \right) \cdot 100$$

$$^n \text{ normalized mol\% } ^{15}\text{N} - \text{DLPC} =$$

$$\text{calc mol\% } ^{15}\text{N} - \text{DLPC} \cdot \sqrt{\left[ \frac{\sigma_{\text{calc mol\% } ^{15}\text{N} - \text{DLPC}}}{\text{calc mol\% } ^{15}\text{N} - \text{DLPC}} \right]^2 + \left[ \frac{\sqrt{[(\sigma_{\text{calc mol\% } ^{15}\text{N} - \text{DLPC}})^2 + (\sigma_{\text{calc mol\% } ^{13}\text{C}_{18} - \text{DSPC}})^2]}}{\text{total calc mol\% lipid}} \right]^2}$$

9	73	104	$7.02 \times 10^{-1}$	$1.07 \times 10^{-1}$	$4.61 \times 10^{-1}$	$5.46 \times 10^{-2}$	70.9	9.5
10	46	120	$3.83 \times 10^{-1}$	$6.65 \times 10^{-2}$	$2.43 \times 10^{-1}$	$2.68 \times 10^{-2}$	39.7	4.8
11	64	112	$5.71 \times 10^{-1}$	$8.95 \times 10^{-2}$	$3.72 \times 10^{-1}$	$4.26 \times 10^{-2}$	58.6	7.5
<b>ROI</b>								
	<b><math>^{12}\text{C}^{15}\text{N}^-</math> cts</b>	<b><math>^{12}\text{C}^-</math> cts</b>	<b><math>^{12}\text{C}^{15}\text{N}^-/^{12}\text{C}^-</math></b>	<b>uncertainty <math>^{12}\text{C}^{15}\text{N}^-/^{12}\text{C}^-</math></b>	<b><math>^{15}\text{N}/^{12}\text{C}</math></b>	<b>uncertainty <math>^{15}\text{N}/^{12}\text{C}</math></b>	<b>calc mol% <math>^{15}\text{N}</math>-DLPC</b>	<b>uncertainty mol% <math>^{15}\text{N}</math>-DLPC</b>
1	17	121	$1.40 \times 10^{-1}$	$3.64 \times 10^{-2}$	$3.36 \times 10^{-3}$	$9.98 \times 10^{-5}$	9.0	0.4
2	36	112	$3.21 \times 10^{-1}$	$6.16 \times 10^{-2}$	$9.02 \times 10^{-3}$	$8.88 \times 10^{-4}$	24.9	2.4
3	36	97	$3.71 \times 10^{-1}$	$7.24 \times 10^{-2}$	$1.06 \times 10^{-2}$	$1.23 \times 10^{-3}$	29.5	3.3
4	22	116	$1.90 \times 10^{-1}$	$4.41 \times 10^{-2}$	$4.89 \times 10^{-3}$	$3.41 \times 10^{-4}$	13.2	1.0
5	10	135	$7.41 \times 10^{-2}$	$2.43 \times 10^{-2}$	$1.28 \times 10^{-3}$	$2.79 \times 10^{-4}$	3.5	0.6
6	14	113	$1.24 \times 10^{-1}$	$3.51 \times 10^{-2}$	$2.84 \times 10^{-3}$	$5.95 \times 10^{-5}$	7.6	0.3
7	26	99	$2.63 \times 10^{-1}$	$5.79 \times 10^{-2}$	$7.18 \times 10^{-3}$	$7.72 \times 10^{-4}$	19.6	2.1
8	3	101	$2.97 \times 10^{-2}$	$1.74 \times 10^{-2}$	$-1.09 \times 10^{-4}$	$4.94 \times 10^{-4}$	0	1.1
9	15	104	$1.44 \times 10^{-1}$	$3.98 \times 10^{-2}$	$3.47 \times 10^{-3}$	$2.08 \times 10^{-4}$	9.3	0.7
10	11	120	$9.17 \times 10^{-2}$	$2.89 \times 10^{-2}$	$1.83 \times 10^{-3}$	$1.35 \times 10^{-4}$	4.9	0.2
11	15	112	$1.34 \times 10^{-1}$	$3.68 \times 10^{-2}$	$3.15 \times 10^{-3}$	$1.13 \times 10^{-4}$	8.4	0.4
<b>ROI</b>								
	<b>calc mol% <math>^{13}\text{C}_{18}</math>-DSPC</b>	<b>Calc mol% <math>^{15}\text{N}</math>-DLPC</b>	<b>total calc mol% lipid</b>	<b>normalized <math>^{13}\text{C}_{18}</math>-DSPC</b>	<b>uncertainty normalized <math>^{13}\text{C}_{18}</math>-DSPC</b>	<b>normalized <math>^{15}\text{N}</math>-DLPC</b>	<b>uncertainty normalized <math>^{15}\text{N}</math>-DLPC</b>	
1	51.2	9.0	60.1	85	8.1	15	1.7	
2	54.2	24.9	79.1	69	8.6	31	4.2	
3	57.2	29.5	86.7	66	9.9	34	5.1	
4	62.5	13.2	75.7	83	10.2	17	2.3	
5	46.0	3.5	49.4	93	7.0	7	1.3	
6	56.4	7.6	63.9	88	9.6	12	1.4	
7	78.7	19.6	98.2	80	14.1	20	3.1	
8	68.3	0	68.1	100	13.3	0	1.6	
9	70.9	9.3	80.2	88	12.7	12	1.6	
10	39.7	4.9	44.6	89	6.5	11	1.3	
11	58.6	8.4	67.0	87	10.0	13	1.6	

**Table S4. Domain C Calculations**

<b>ROI</b>	<b><math>^{13}\text{C}^1\text{H}^-</math> cts</b>	<b><math>^{12}\text{C}^-</math> cts</b>	<b><math>^{13}\text{C}^1\text{H}^-/^{12}\text{C}^-</math></b>	<b>uncertainty <math>^{13}\text{C}^1\text{H}^-/^{12}\text{C}^-</math></b>	<b><math>^{13}\text{C}/^{12}\text{C}</math></b>	<b>uncertainty <math>^{13}\text{C}/^{12}\text{C}</math></b>	<b>calc mol% <math>^{13}\text{C}_{18}</math>-DSPC</b>	<b>uncertainty mol% <math>^{13}\text{C}_{18}</math>-DSPC</b>
1	61	121	$3.47 \times 10^{-1}$	$5.44 \times 10^{-2}$	$2.18 \times 10^{-1}$	$1.86 \times 10^{-2}$	35.8	3.4
2	58	111	$4.22 \times 10^{-1}$	$6.84 \times 10^{-2}$	$2.70 \times 10^{-1}$	$2.82 \times 10^{-2}$	43.7	5.1
3	63	134	$3.11 \times 10^{-1}$	$4.75 \times 10^{-2}$	$1.94 \times 10^{-1}$	$1.38 \times 10^{-2}$	32.0	2.6
4	70	114	$6.58 \times 10^{-1}$	$9.99 \times 10^{-2}$	$4.31 \times 10^{-1}$	$4.97 \times 10^{-2}$	66.9	8.7
5	54	120	$2.90 \times 10^{-1}$	$4.75 \times 10^{-2}$	$1.79 \times 10^{-1}$	$1.39 \times 10^{-2}$	29.8	2.6
6	70	118	$3.94 \times 10^{-1}$	$5.95 \times 10^{-2}$	$2.51 \times 10^{-1}$	$2.20 \times 10^{-2}$	40.8	4.0

7	68	100	$4.29 \times 10^{-1}$	$6.75 \times 10^{-2}$	$2.75 \times 10^{-1}$	$2.75 \times 10^{-2}$	44.5	4.9
8	57	133	$2.68 \times 10^{-1}$	$4.24 \times 10^{-2}$	$1.64 \times 10^{-1}$	$1.04 \times 10^{-2}$	27.4	2.0
9	45	121	$2.42 \times 10^{-1}$	$4.22 \times 10^{-2}$	$1.47 \times 10^{-1}$	$1.03 \times 10^{-2}$	24.6	2.0
10	58	124	$3.34 \times 10^{-1}$	$5.31 \times 10^{-2}$	$2.09 \times 10^{-1}$	$1.77 \times 10^{-2}$	34.5	3.3
11	55	118	$2.74 \times 10^{-1}$	$4.47 \times 10^{-2}$	$1.68 \times 10^{-1}$	$1.19 \times 10^{-2}$	28.1	2.3
12	61	126	$3.82 \times 10^{-1}$	$5.96 \times 10^{-2}$	$2.42 \times 10^{-1}$	$2.21 \times 10^{-2}$	39.5	4.0
13	60	110	$3.38 \times 10^{-1}$	$5.42 \times 10^{-2}$	$2.12 \times 10^{-1}$	$1.84 \times 10^{-2}$	34.9	3.4
<b>ROI</b>								
	<b><math>^{12}\text{C}^{15}\text{N}^-</math> cts</b>	<b><math>^{12}\text{C}^-</math> cts</b>	<b><math>^{12}\text{C}^{15}\text{N}^-/^{12}\text{C}^-</math></b>	<b>uncertainty <math>^{12}\text{C}^{15}\text{N}^-/^{12}\text{C}^-</math></b>	<b><math>^{15}\text{N}/^{12}\text{C}</math></b>	<b>uncertainty <math>^{15}\text{N}/^{12}\text{C}</math></b>	<b>calc mol% <math>^{15}\text{N}</math>-DLPC</b>	<b>uncertainty mol% <math>^{15}\text{N}</math>-DLPC</b>
1	18	121	$4.40 \times 10^{-1}$	$1.11 \times 10^{-1}$	$1.27 \times 10^{-2}$	$2.44 \times 10^{-3}$	36.1	6.5
2	8	111	$1.24 \times 10^{-1}$	$4.54 \times 10^{-2}$	$2.84 \times 10^{-3}$	3.80E-04	7.6	1.1
3	15	134	$1.55 \times 10^{-1}$	$4.22 \times 10^{-2}$	$3.81 \times 10^{-3}$	2.82E-04	10.2	0.9
4	7	114	$1.18 \times 10^{-1}$	$4.60 \times 10^{-2}$	$2.65 \times 10^{-3}$	3.99E-04	7.1	1.2
5	40	120	$5.30 \times 10^{-1}$	$9.67 \times 10^{-2}$	$1.55 \times 10^{-2}$	$1.99 \times 10^{-3}$	44.9	5.3
6	6	118	$1.34 \times 10^{-1}$	$5.62 \times 10^{-2}$	$3.16 \times 10^{-3}$	$7.20 \times 10^{-4}$	8.4	2.0
7	4	100	$5.25 \times 10^{-2}$	$2.68 \times 10^{-2}$	$6.04 \times 10^{-4}$	$2.01 \times 10^{-4}$	1.7	0.4
8	25	133	$2.92 \times 10^{-1}$	$6.37 \times 10^{-2}$	$8.11 \times 10^{-3}$	$9.56 \times 10^{-4}$	22.2	2.6
9	24	121	$2.82 \times 10^{-1}$	$6.31 \times 10^{-2}$	$7.80 \times 10^{-3}$	$9.36 \times 10^{-4}$	21.3	2.6
10	11	124	$7.71 \times 10^{-2}$	$2.43 \times 10^{-2}$	$1.37 \times 10^{-3}$	$2.80 \times 10^{-4}$	3.7	-0.6
11	12	118	$1.66 \times 10^{-1}$	$5.04 \times 10^{-2}$	$4.16 \times 10^{-3}$	$5.37 \times 10^{-4}$	11.1	1.5
12	24	126	$3.14 \times 10^{-1}$	$6.99 \times 10^{-2}$	$8.78 \times 10^{-3}$	$1.15 \times 10^{-3}$	24.2	3.1
13	15	110	$1.44 \times 10^{-1}$	$3.96 \times 10^{-2}$	$3.46 \times 10^{-3}$	$2.01 \times 10^{-4}$	9.2	0.7
<b>ROI</b>								
	<b>calc mol% <math>^{13}\text{C}_{18}</math>-DSPC</b>	<b>calc mol% <math>^{15}\text{N}</math>-DLPC</b>	<b>total calc mol% lipid</b>	<b>normalized <math>^{13}\text{C}_{18}</math>-DSPC</b>	<b>uncertainty normalized <math>^{13}\text{C}_{18}</math>-DSPC</b>	<b>normalized <math>^{15}\text{N}</math>-DLPC</b>	<b>uncertainty normalized <math>^{15}\text{N}</math>-DLPC</b>	
1	35.8	36.1	71.9	50	5.0	50	10.4	
2	43.7	7.6	51.3	85	6.7	15	2.7	
3	32.0	10.2	42.2	76	3.4	24	2.6	
4	66.9	7.1	73.9	90	11.8	10	2.0	
5	29.8	44.9	74.7	40	3.5	60	8.6	
6	40.8	8.4	49.3	83	5.5	17	4.4	
7	44.5	1.7	46.2	96	6.9	4	0.9	
8	27.4	22.2	49.7	55	2.7	45	6.0	
9	24.6	21.3	45.9	54	2.7	46	6.5	
10	34.5	3.7	38.2	90	4.4	10	1.7	
11	28.1	11.1	39.2	72	3.0	28	4.4	
12	39.5	24.2	63.7	62	5.1	38	5.7	
13	34.9	9.2	44.2	79	4.4	21	2.2	

**References**

1. C. Galli Marxer, M. L. Kraft, P. K. Weber, I. D. Hutcheon, S. G. Boxer, *Biophys. J.* **88**, 2965 (2005).
2. M. L. Kraft et al., *Appl. Sur. Sci. in press*, doi:10.1016/j.apsusc.2006.02.116 (2006).